www.czasopisma.pan.pl PAN www.journals.pan.pl

ARCHIVES of FOUNDRY ENGINEERING

ISSN (2299-2944)
Volume 2025
Issue 1/2025

59 – 74

10.24425/afe.2025.153775

8/1

Published quarterly as the organ of the Foundry Commission of the Polish Academy of Sciences

Analysis of the Applicability of Heat Treatment of EN AC-46000 Alloy Castings Made with Vacuum-Assisted HPDC Technology

T. Szymczak [a, *], B. Pisarek [a], B. Januszewicz [b], M. Różycka [a]

[a] Department of Materials Technology and Production Systems, Lodz University of Technology, Stefanowskiego 1/15, 90-537 Łódź, Poland

[b] Institute of Materials Engineering, Lodz University of Technology, Stefanowskiego 1/15, 90-537 Łódź, Poland

* Corresponding author: E-mail address: tomasz.szymczak@p.lodz.pl

Received 06.11.2024; accepted in revised form 27.12.2024; available online 17.03.2025

Abstract

The aim of the study was optimization of the technological parameters of the thermal treatment of EN AC-46000 alloy products made in the vacuum aided HPDC technology in the function of simultaneous maximization of the alloy's mechanical properties with no deformation of the cast's surface. The produced casts were subjected to thermal treatment T6 according to the elaborated experiment plan. The samples were examined in respect of selected mechanical properties as well as the presence of deformation on the castings surfaces. Also performed was an analysis of the castings microstructure as well as optimization of the technological parameters of the supersaturation and ageing process by means of statistical methods, i.e. the Box-Wilson optimization method (Stage I) and stepwise multiple regression in the Statgraphics software (Stage II). Also, a simulation was carried out, predicting the mechanical properties for the specific supersaturation and ageing parameters, from which optimized values of the setpoints of both processes were obtained. The study presents the results of validation tests of pressure casts subjected to thermal treatment performed according to the previously determined optimal parameters of supersaturation and ageing. These results confirmed the effectiveness of the conducted precipitation hardening treatment.

Keywords: Heat treatment, Mechanical properties, EN AC-46000 alloy, VHPDC, Multi-criteria optimization

1. Introduction

The studies [1-7] present the results of tests referring to heat treatment in the form of precipitation hardening of die multi-component Al-Si alloys die-cast into a sand mould. These studies investigate multi-component hypo- and near-eutectic Al-Si alloys. The content of the most crucial alloy elements in these investigations was within the scope of: 6–13% Si; 0.57–3.70% Cu and 0.2–1.1% Mg. The solid solution α_{Al} supersaturation was carried out by way of cooling the alloy in water right after the annealing. The solution annealing temperature equalled t_p=490–540°C and the annealing time τ_p was within the scope of 1–10 hrs. Artificial ageing was applied in the temperature scope of t_s=150–210°C and the time of τ_s=5–100 hrs, where the most

frequently applied ageing time was within the scope of 5–8 hrs. The provided ageing time of 100 hrs refers to a single ageing procedure test, described in [3], applied for an extremely low temperature value of 150°C. A properly performed thermal treatment led to an increase of the fundamental strength properties of the alloy at the cost of the acceptable reduction of its plastic properties. However, depending on the alloys' chemical composition and the casting conditions, different values of the fundamental parameters of the thermal treatment process t_p, τ_p, t_s and τ_s gave, in effect, the optimal properties of the alloy after this treatment.

In turn, Al-Si alloy casts made in the HPDC technology are not normally subjected to thermal treatment under industrial conditions. The biggest problem connected with precipitation hardening of Al-Si alloys pressure casts is their relatively high gassing level compared to other casting technologies. As given by the authors of [8, 9], the average gas content in pressure casts made of Al alloys is higher than 10 cm^3/100 g. The main sources of the presence of gas porosities in an alloy are hydrogen absorption and introduction of air into the cast during the casting process. The source of H_2 in Al alloys are processes conducted in ambient temperature, such as: alloy melting, operations of pouring the liquid alloy from the melting furnace into the transfer ladle, and then from this ladle into the HPDC machine furnace, and a prolonged time of isothermal retention of the liquid alloy in the HPDC machine furnace. A reduction of hydrogen absorption can be achieved because of refinement of the liquid alloy [10]. On the other hand, the source of air bubbles in HPDC casting is generally due to improper piston travel speed in the pressing chamber, which leads to mixing of liquid metal and air.

The high gassing level of castings made in the traditional HPDC technology during the solution annealing process conducted at high temperatures causes expansion of gas bubbles. The effect of this are two tapes of pressure cast defects [11]:

1) Surface spalling or surface bubbles (blistering) of the casts caused by the gas pressure in the pores present directly at the surface of the cast.
2) Deformation of the cast's shape, its swelling.

An exemplary pressure cast with visible blistering has been shown in Fig. 1.

Fig. 1. Exemplary pressure die cast with visible blistering [own study]

The sub-pressure in the pressure mould equalling 500–100 mbar should reduce the number of air bubbles in the cast. The authors of [8,9] report that aiding the HPDC process with vacuum causes gassing like that of casting into sand moulds and dies. In such a case, the obtained gassing level of an Al alloy cast is at the level of about 5 to below 1 cm^3/100 g.

The results of tests related to the precipitation hardening of Al-Si alloys die casts produced in the traditional pressure casting process are presented in the studies [8, 12–14]. These studies assume that, to carry out solution annealing of pressure casts, the process parameters values should be lowered. The studies [8, 12, 13] examine the effectiveness of precipitation hardening of a pressure cast Al-Si alloy Al-(7.5–12)Si-(1.5–4.5)Cu-(≤1.3)Fe-(≤0.5)Mn-(≤3.0)Zn-(≤0.75)Mg-(≤1.5) other elements. The applied solution annealing temperature was within the scope of 440–530°C, and the annealing time was 10–120 min. Due to the presence of surface defects (blistering), the temperature and time of the process were limited to ≤490°C and ≤15 min, respectively. Right after the described annealing process, supersaturation of the alloy in water was carried out, followed by an artificial ageing treatment (T6). The ageing was examined at a temperature from the scope of 150–210°C and at a time of up to 100 hrs. It was demonstrated that, because of conducting a whole process of precipitation hardening, it is possible to obtain tensile strength UTS of the silumin at the level of 400 MPa and its yield stress YS above 300 MPa. The study [14] presents the results of precipitation hardening tests of a pressure cast alloys Al-(9)Si-(3,5)Cu-(0.1–1.0)Fe-(0.5)Mn-(0.3)Mg. In this case, the applied solution annealing parameters were 510°C/30 min, and the ageing temperature was 170°C within the time of up to 35 hrs. After a complete thermal treatment (T6), similar results were obtained to those in the previously described studies, i.e. UTS≈400 MPa and YS>300 MPa. The study does not mention the effect of the applied solution annealing conditions on the presence of surface defects of the castings. In can be inferred from the data included in the studies [8, 12–14] that the safe solution annealing parameters for traditionally produced casts under high pressure are temperature of t_p=490°C and time of τ_p=15 min. In turn, in the case of ageing, the application of low temperature values t_s of the process causes a prolongation of its time τ_s. For example, Table 1 shows the values of temperature t_s and time τ_s for which the optimal UTS values of the examined multi-component Al-Si alloys were obtained.

Table 1.
Exemplary artificial ageing parameters providing the optimal UTS values

Artificial ageing parameters	
Temperature t_s, °C	Time τ_s, hr.
150	~ 20
170	~ 10
210	~ 0.5

Considering that aiding pressure casting with vacuum significantly lowers the gassing level of the casts compared to the traditional pressure casting technology, and which is comparable to casting into sand moulds and dies, for a fuller application of the possibilities of precipitation hardening, it seems justifiable to

examine in a broader scope the temperature ands time of solution annealing in respect of the values of 490°C and 15 min.

And so, the aim of the research is to optimize the technological parameters of the process of precipitation hardening of EN AC-46000 alloy casts made in the pressure casting technology aided with vacuum in the function of a simultaneous maximization of the mechanical properties of the alloy, with no surface deformation of the cast.

2. Test methodology

2.1. Production of test casts

For the tests, an EN AC-46000 alloy was used as the base alloy [15]. Its chemical composition scope has been shown in Table 2.

Table 2.
Chemical composition scope of the EN AC-46000 alloy used in the tests

Chemical composition, % wt.											
Si	Cu	Zn	Fe	Mg	Mn	Ni	Cr	Ti	Sr	B	Al
9.45–9.76	2.03–2.10	0.71–0.74	0.70–0.75	0.21–0.23	0.27–0.28	0.062–0.069	0.028–0.030	0.073–0.077	0.020–0.021	0.010–0.012	residue

The alloy was refined with the use of solid refiners Ecosal, Ecremal and Desydral, as well as modified with an addition of Sr and TiB. The project where the research presented in this paper was carried out also included the effect of TiB modification on changes in the microstructure of the alloy and, consequently, its properties as well. The results showed that TiB further increases the grain size refinement in HPDC technology. The base alloy was melted in a gas heated shaft furnace with a capacity of 1,5 ton. Inside the shaft furnace, the alloy was refined with the solid refiner Ecosal Al113.S. After the melting and refining, the alloy was deslagged and transported to a heating furnace set up near the pressure machine.

The EN AC-46000 alloy casts from which the test samples were prepared had been produced in the foundry of the Wifama-Prexer company. These casts had the form of "crosses" (Fig. 2), which were cast in a two-chamber casting mould in the technology of vacuum assisted die casting (VADC). Their average wall thickness was ~5 mm. Together with the "crosses", strength tests samples were also cast. These were flat samples with a rectangular cross-section and the dimensions of 3,5/10,5 mm. The castings were made on a pressure machine with a cold horizontal pressure chamber Idra 900CS. The parameters of the casting process are a trade secret of the foundry. The pressure machine was equipped with a device for producing sub-pressure in the casting mould. The sub-pressure obtained in the mould equalled 500 mbar.

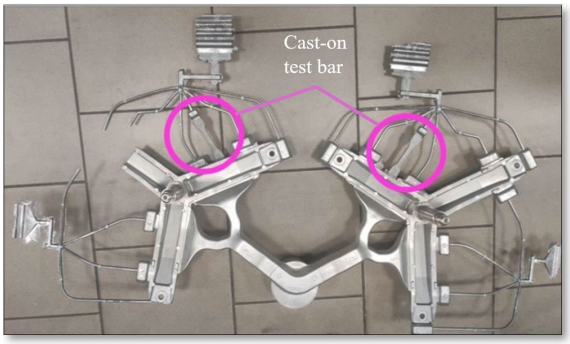

Fig. 2. View of the "cross" casts together with the casts for the strength tests [own study]

2.2. Thermal treatment T6

Both the process of supersaturation and ageing were conducted with the use of a muffle furnace produced by Snol, presented in Fig. 3.

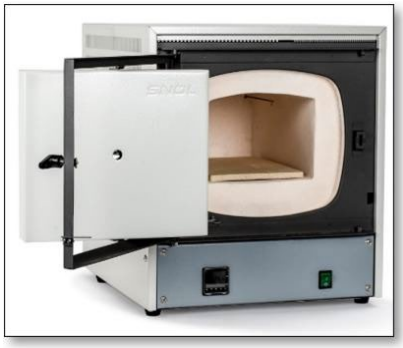

Fig. 3. A muffle furnace produced by SNOL 8,2/1100 LSM01

The program of the furnace was set to the specified temperature according to the experiment plan. After reaching the desired temperature, the samples were placed into it. Next, after the designated solution annealing time had passed, the samples were cooled in water at room temperature, which ensured the occurrence of supersaturation. After the ageing process, the samples underwent natural cooling at room temperature. The temperature values of solution annealing t_p and ageing t_s, as well as the times of these procedures τ_p and τ_s have been shown in the experiment plan.

2.3. Microstructure tests

On samples collected from pressure casts, microsections were made and their surfaces were etched with 2% water solution of HF acid. The microsections prepared this way were observed, and microstructure images were taken on a metallographic microscope Nikon Eclipse MA200 equipped with a digital camera Nikon DS-Fi 1. The photographs were recorded with the use of the digital image analysis software NIS-Elements Advanced Research.

The tests of the chemical composition on the sample microsections' surfaces were conducted by the X-ray

microanalysis method EDS – X-ray energy dispersion. For the tests, a scanning microscope JEOL JSM-6610LV was used, integrated with the MiniCL-GATAN Cathodoluminescence Imaging System and Oxford Instruments EDS X-MAX 80 systems as well as the backscattered electron acquisition system EBSD NordlysMax. The examinations were carried out by means of the EDS AZtecEnergy software.

The examined samples were placed in the microscope's chamber and the optimal test parameters were determined, i.e.: working distance 10 mm, accelerating voltage 20 kV, beam current 60, analysis time 120 seconds. The chemical composition analysis was made for the total surface presented in the photograph.

2.4. Determination of fundamental mechanical properties

The values of tensile strength UTS, yield stress YS and relative elongation A_{gt} were determined in a static tension test on a testing machine Instron 4485. The test was conducted according to the norm PN-EN ISO 6892-1:2016 [16]. The applied strain rate was R=6 MPa/s and the deformation rate were 0.0008 m/s. The test samples were collected from the prepared pressure casts (Fig. 3). Within the measuring section, they had a rectangular cross-section with the dimensions of 3.5/10.5 mm. For each analyzed experiment, 3 samples were examined. The hardness measurement of the tested alloys was conducted by the Brinell method according to the norm PN-EN ISO 6506-1:2014-12 – Polish version [17]. In this method, a tungsten carbide ball was used as the indenter. The hardness measurement was conducted on metallographic cross-sections. The load was chosen so that the indentation diameter d would be within the scope of $0.24\ D < d < 0.6\ D$. The diameter of the ball was D=2.5 mm, the load was 613 N, and the static load holding time was 30 s.

2.5. Optimization of thermal treatment parameters

The general model of the experiment has been presented in Figure 4.

The inputs in the experiment are four factors.

- supersaturation temperature (t_p,°C),
- supersaturation time (τ_p, h.),
- ageing temperature (t_s,°C),
- ageing time (τ_s, h.).

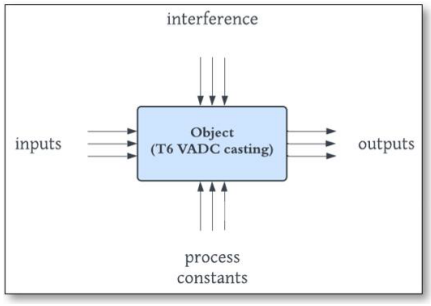

Fig. 4. General experiment model [own study]

The experiment also includes five outputs, constituted by the following properties:

- ultimate tensile strength (UTS),
- yield stress (YS),
- relative elongation at maximal force (A_{gt}),
- hardness (HB),
- presence of deformation on the cast's surface (DCS).

The constant process parameters are those which did not change for the entire duration of the experiment. They include e.g.: the muffle furnace, the number of details placed in the furnace for thermal treatment, or the container with cold water, and the water temperature as a constant parameter of the supersaturation stage. In turn, disturbances are immeasurable phenomena, which can affect the input parameters in an uncontrolled and unpredictable way. An example of such a disturbance is a voltage spike in the power grid or an internal fault in the furnace.

The experiment planning was based on the Box-Wilson optimization method, which involves searching for the minimum or maximum response of the object to the given inputs.

This method minimizes the number of experiments which should be performed to obtain the extreme response of the object as quickly as possible. The total number of tasks "n" to be performed in the experiment (around the central point and for that point) is determined with the use of the formula (1):

$$n=2^s+1 \tag{1}$$

where:

s – number of inputs (s=4),

1 – corresponds to a single task for the central task parameters (D0).

After substituting the data into the equation (1), the following was obtained:

$n=2^4+1=17$.

The optimization of the parameters for the thermal treatment T6 was carried out in two stages.

The first stage involved planning tasks in the experiment at two levels around the central point. Figure 5 shows the spatial model of the experimental design.

After establishing the scope of acceptable input factor values, a plan of the experiment was prepared, shown in Table 3. According to Box-Wilson's two-stage experiment planning method, the values of the upper ($X_i^0+\Delta X_i$) and lower ($X_i^0-\Delta X_i$) parameter level were assigned to the corresponding tasks. As the output values Y_i the following were examined: UTS, YS, A_{gt}, HBW, DSC.

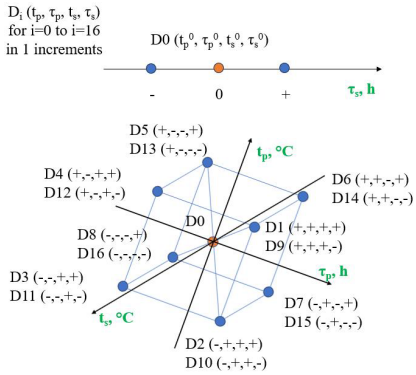

Fig. 5. General experiment model [own study]

Table 3.
Experiment model [own study]

	X_i				Y_i
	t_p, °C	τ_p, h	t_s, °C	τ_s, h	
Range X_i	490–540	1–11	150–200	4–12	
X_i^0 (D0)	515	6	175	8	
ΔX_i	25	5	25	4	
X_i^0-ΔX_i	(-) 490	(-) 1	(-) 150	(-) 4	
X_i^0+ΔX_i	(+) 540	(+) 11	(+) 200	(+) 12	
Runs					
D1	(+) 540	(+) 11	(+) 200	(+) 12	
D2	(-) 490	(+) 11	(+) 200	(+) 12	
D3	(-) 490	(-) 1	(+) 200	(+) 12	
D4	(+) 540	(-) 1	(+) 200	(+) 12	
D5	(+) 540	(-) 1	(-) 150	(+) 12	
D6	(-) 490	(+) 11	(-) 150	(+) 12	
D7	(-) 490	(+) 11	(-) 150	(+) 12	
D8	(-) 490	(-) 1	(-) 150	(+) 12	
D9	(+) 540	(+) 11	(+) 200	(-) 4	
D10	(-) 490	(+) 11	(+) 200	(-) 4	
D11	(-) 490	(-) 1	(+) 200	(-) 4	
D12	(+) 540	(-) 1	(+) 200	(-) 4	
D13	(+) 540	(-) 1	(-) 150	(-) 4	
D14	(+) 540	(+) 11	(-) 150	(-) 4	
D15	(-) 490	(+) 11	(-) 150	(-) 4	
D16	(-) 490	(-) 1	(-) 150	(-) 4	

At the first optimization stage, the vector of the most intensive changes in the object's response Y^i to the given inputs X^i was searched for, lying on the plane described by the equation (2):

$$Y_i=f(t_p, \tau_p, t_s, \tau_s)=a_0+a_1\cdot t_p+a_2\cdot\tau_p+a_3\cdot t_s+a_4\cdot\tau_s \quad (2)$$

For the particular planes, the gradient vector was determined according to the equation (3):

$$\nabla f=(\partial f/\partial t_p, \partial f/\partial\tau_p, \partial f/\partial t_s, \partial f/\partial\tau_s) \quad (3)$$

In determining the particular derivatives, the gradient vector for the function (2) can be expressed as follows $\nabla f=(a_1, a_2, a_3, a_4)$.

The resultant vector for the planes (2) can be determined from the equation (4):

$$\nabla f=(\Sigma a_1, \Sigma a_2, \Sigma a_3, \Sigma a_4) \quad (4)$$

where:

$\Sigma a_i=a_{i\_UTS}+a_{i\_YS}+a_{i\_Agt}+a_{i\_HBW}$.
$i=\{1, 2, 3, 4\}$

At the second stage of optimization, based on the selected tasks, a mathematical description of the changes in the object's response Y_i to the given inputs X_i was searched for in the form of a regression function (5) (a function with a single extremum):

$$Y_i=f(t_p,\ \tau_p,\ t_s,\ \tau_s)=a_0+a_1\cdot t_p+a_2\cdot\tau_p+a_3\cdot t_s+a_4\cdot\tau_s+a_5\cdot t_p\cdot\tau_p+$$
$$+a_6\cdot t_p\cdot t_s+a_7\cdot t_p\cdot\tau_s+a_8\cdot\tau_p\cdot t_s+a_9\cdot\tau_p\cdot\tau_s+a_{10}\cdot t_s\cdot\tau_s \quad (5)$$

The relation (5) was determined for the central task and the tasks after which no surface deformation of the cast occurred, with the use of the method of stepwise multiple regression analysis, either with the "forward" or "backward" method, with or without the constant term (a_0). The determined equations were:

- significant $F_{model}>F_{kryt}=F(\alpha, \upsilon_1, \upsilon_2)$ (F –Fisher's test; α – assumed significance level; υ_1, υ_2 – degrees of freedom for the critical test F; υ_1=n-k-1; υ_2=n; n – number of tasks whose results were used to determine the relation (3); k – number of terms in the equation (5) in which input variables are present X_i; 1 – considered when coefficient a_0) is present in the equation (5).
- with significant coefficients of the regression function ($p_{\_value\_}a_i\leq\alpha$),
- with the highest possible coefficient R^2 ($R^2\rightarrow 1$),
- with the lowest possible standard deviation SEE→min,
- with the lowest possible mean absolute error MAE→min.

In order to make it possible to compare the results for the object's response to the given inputs, their normalization was carried out (nY_i) , with the assumption that the responses of UTS, YS, A_{gt}, HBW are stimulants (the higher the response's value, the better), according to the equation (6):

$$nY_i=(Y_i-Y_i\_min)/(Y_i\_max-Y_i\_min) \quad (6)$$

For the object's response to the given inputs Y_i=DSC, the values DSC=1 was assumed when, after the thermal treatment T6, deformation of the cast's surface was observed, while DSC=0 – in a case when no surface deformation occurred. For such assumptions, the response of DSC is a destimulant (the lower the response's value, the better). Its normalized values were determined from the equation (7):

$$nY_i=(Y_i\_max-Y_i)/(Y_i\_max-Y_i\_min) \quad (7)$$

The optimization criterion was described by the relation Fo (8):

$$Fo = nUTS + nYS + nAt + nHBW \rightarrow max \text{ for } nDCS=l\ (DCS=0) \quad (8)$$

The sequence of steps realized during the optimization of thermal treatment T6 of alloy EN AC-46000 was as follows:

Stage I – elaboration of the experiment plan, realization of the tasks in the experiment, measurements of the mechanical properties of the test samples, identification of the DCS index on the cast sample, for the responses of UTS, YS A_{gt}, HBW, determination of the planes described by the relation (2), identification of the vectors of the most intensive changes of the object's response Y_i to the given inputs X_i, determination of the resultant vector, elaboration of the experiment plan – tasks lying in the direction determined by the resultant vector.

Stage II – based on the object's response Y_i for the tasks: D0, tasks lying in the direction determined by the resultant vector and the tasks from Stage 1 for which the index DSC=0, determination of the regression function (5), in the scope of the input parameters variability X_i, tabulation of the regression function (5), determination of the normalized values nX_i, calculation of the objective function value Fo, identification of the input factors' values X_i (t_p, τ_p, t_s, τ_s) for which the objective function Fo (8) reaches the maximum – end of optimization.

3. Experiment results

The experiment results presented above include: microstructure tests of the analyzed alloy EN AC-46000, both in its as-cast state (not subjected to thermal treatment T6) and after the thermal treatment T6, as well as actions carried out in Stages I and II of optimization.

3.1. Microstructure tests

The microstructure of the pressure-cast EN AC-46000 alloy recorded with the use of a scanning microscope, as well as the distribution maps of the main alloying elements in the examined areas, are presented in Fig. 6 (a, b).

In both analyzed areas, there are spots with an increased concentration of Al, which correspond to the solid solution dendrites α_{Al}. Areas characterizing in a high concentration of Si are in the double eutectic area $\alpha_{Al}+\beta(Si)$ and they are eutectic silicon precipitates with a morphology similar to a plate-like structure. In Fig. 7(a), we can see an area with a high concentration of Fe, Mn and Cr, as well as an increased concentration of Al and Si, which is probably similar to a wall-like precipitate of phase $Al_{15}(Fe, Mn, Cr)_3Si_2$. In turn, in area 2, next to dendrites of phase α_{Al} and a double eutectic, there are areas with an increased concentration of Cu, which constitute precipitates of the intermetallic phase Al_2Cu, commonly occurring in multicomponent Al-Si alloys. The microstructure of the examined alloy was thoroughly analyzed in the studies [18–24]. The data presented there indicate consistency with the microstructure description provided above by the author. These studies also confirmed the possibility of occurrence in alloy EN AC-46000 of phase Mg_2Si, or other more complex phases from the Al-Cu-Mg-Si system (e.g. $Al_8CuMg_8Si_6$ and $Al_5Cu_2Mg_8Si_6$) and the Al-Mg-Fe-Si system ($Al_8Mg_3FeSi_6$).

a)

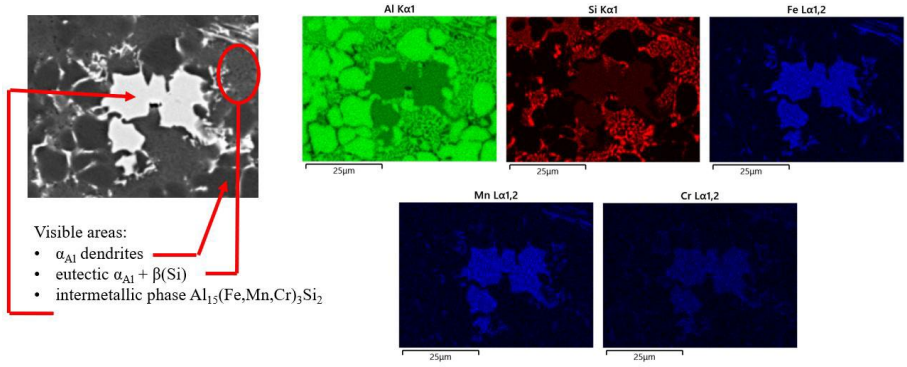

b)

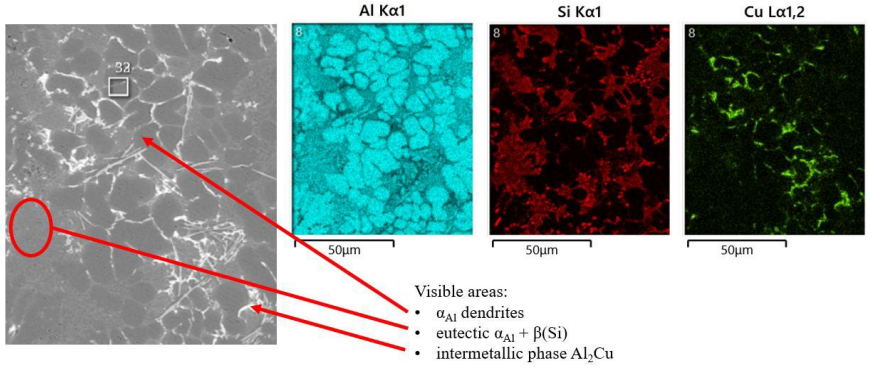

Fig. 6. Microstructure of the pressure-cast EN AC-46000 alloy without a thermal treatment and the distribution maps of the basic elements in the selected alloy areas: a) area 1; b) area 2

Figure 7 shows an example microstructure of the EN AC-46000 alloy after the thermal treatment T6, along with the concentration maps of Al, Si, Fe, and Mn in the examined area.

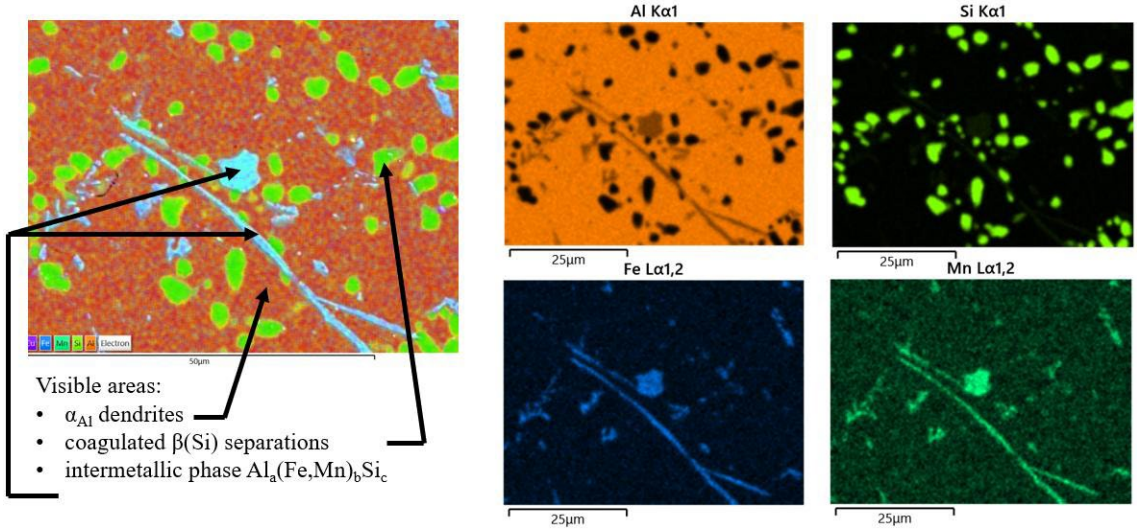

Fig. 7. Exemplary microstructure of the pressure-cast EN AC-46000 alloy after the thermal treatment T6 and the distribution maps of Al, Si, Fe and Mn in the examined area.

The presented data indicates that the matrix of the alloy after the thermal treatment T6 is constituted by a solid solution α_{Al}, and the eutectic silicon precipitates underwent the coalescence and coagulation processes described in the literature [8, 11, 14, 25-27]. As a result of the mentioned processes, the number of β(Si) precipitates decreased in favor of an increase in their size, and their shape also changed to become significantly more compact. In contrast, the intermetallic phase precipitates present in the alloy did not undergo significant transformations. To better highlight the elements of the microstructure of the studied alloy, representative areas were photographed with the use of an optical microscope. The microstructure of the pressure-cast EN AC-46000 alloy in its as-cast state (not subjected to thermal treatment) and for specific variants of thermal treatment T6 has been presented in Figures 8-10.

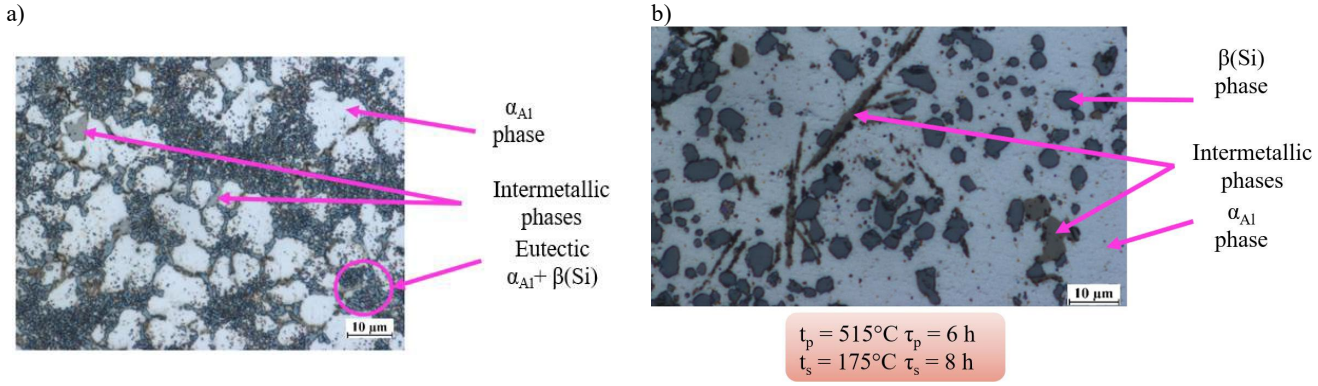

Fig. 8. Exemplary microstructure of the pressure-cast EN AC-46000 alloy (task D0): a) without thermal treatment and b) after thermal treatment T6 (experiment D0)

Figure 8a shows the microstructure of the initial pressure-cast EN AC-46000 alloy. This microstructure consists of primary α_{Al} phase dendritic precipitates, fine-grained α_{Al} + β(Si) eutectic, and intermetallic phases. The intermetallic phase precipitates shown in the figure have a compact morphology, either block-like or resembling a wall structure, as well as a needle-like form.

Figure 8b shows the microstructure of the examined alloy after the precipitation hardening process conducted according to the specifications for point D0 in the experiment plan (this is the so-called central point). Solution treatment was carried out after annealing at the temperature of 515°C for the time of 6 hours. The aging temperature and time were 175°C and 8 hours, respectively.

It is well-known that aging does not cause significant changes in the microstructure of aluminium alloys. In contrast, solution treatment leads to the coagulation and coalescence of silicon precipitates. Consequently, the microstructure presented in the figure consists of a matrix in the form of a solid solution of α_{Al}, along with coagulated β(Si) precipitates and intermetallic phases, which did not significantly change in morphology compared to the alloy in its as-cast state.

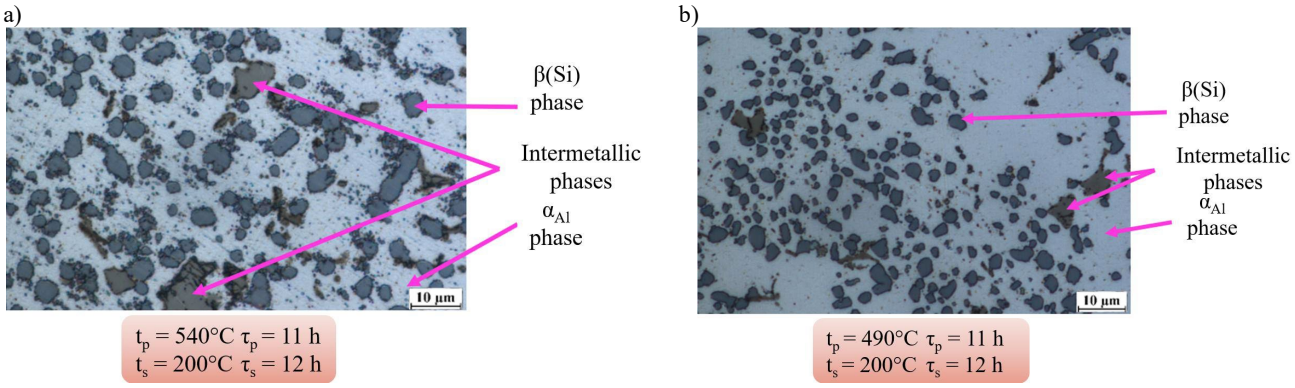

Fig. 9. Exemplary microstructure of the pressure-cast EN AC-46000 alloy after thermal treatment T6: a) task D1 and b) task D2

Figure 9a shows the microstructure of the alloy after solution treatment conducted at the temperature of 540°C for 11 hours, while aging occurred at 200°C for the time of 12 hours (task D1). These aging conditions are also analogical to those for the subsequent analyzed microstructures. The microstructure presented is like the one previously shown, obtained for the central point of the experiment.

The next analyzed microstructure shown in Figure 10b refers to task D2 (t_p=490°C and τ_p=11 hrs.). In this case, the microstructure of the alloy is very similar to the previously described microstructures from tasks D0 (Figure 8b) and D1 (Figure 9a).

Figure 10a shows the microstructure of the alloy for task D3. In this case, extremely low values of the solution treatment parameters were applied, that is the temperature of 490°C and the time of 1 hour. The microstructure image indicates that the silicon precipitates did not undergo coalescence and coagulation processes. The resulting microstructure is like that in the as-cast state. It is likely that the solution treatment time was too short for the mentioned processes to occur.

Figure 10b presents the microstructure of the alloy for experiment D4, in which a solution treatment time of 1 hour was also applied, with the temperature of this operation equalling 540°C.

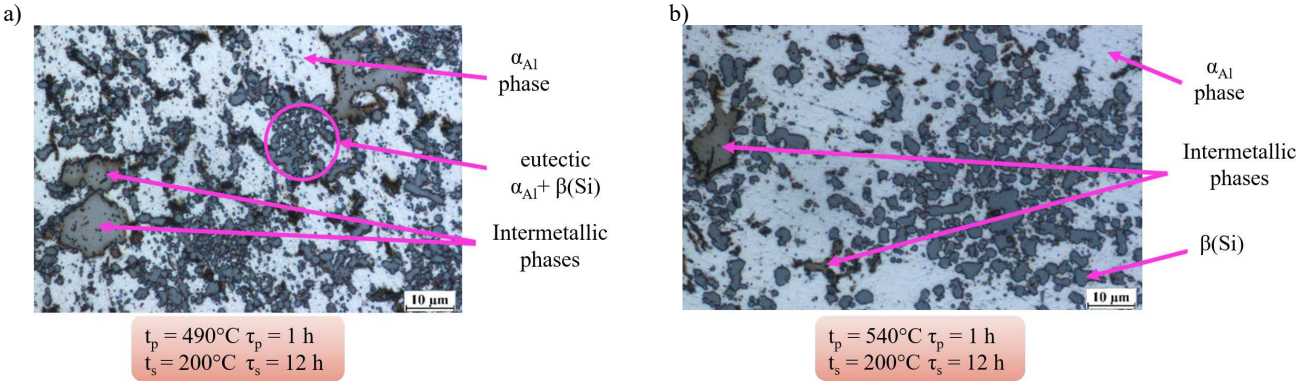

Fig. 10. Exemplary microstructure of a pressure-cast EN AC-46000 alloy after thermal treatment T6: a) task D3 and b) task D4

The microstructure image clearly shows that the provided conditions made it possible for the coagulation and coalescence processes of the silicon precipitates to take place. The microstructure obtained in this case is like those achieved in tasks D0 (Figure 8b), D1 (Figure 9a), and D2 (Figure 9b).

3.2. Results of tests of the alloy's fundamental mechanical properties

Table 4 shows a compilation of the test results for the fundamental mechanical properties of an EN AC-46000 alloy cast in the technology of vacuum assisted pressure casting. The strength

tests were conducted for casts subjected to precipitation hardening carried out according to the experiment plan for the first step of optimization.

The highest values of the examined individual mechanical properties were obtained for different settings of the thermal treatment parameters. The highest tensile strength value UTS=352 MPa was reached in the central point D0 of the experiment plan. Relatively high UTS values were also achieved for the extremely high ageing parameters (t_s=200°C i τ_s=12 hrs). In turn, the lowest values UTS=(225–247) MPa were recorded with the maximal saturation temperature and time (t_p=540°C and τ_p=11 hrs).

The highest yield stress value YS=309 MPa was obtained in the central point D0, as in the case of UTS. We can also notice clearly higher YS values with the maximal ageing temperature t_s=200°C, compared to the tasks with the extremely low temperature t_s=150°C. The lowest values YS≤198 MPa were achieved in the experiments with the application of ageing at t_s=150°C for the time of τ_s=4 hours. Relative elongation A_{gt} reached its highest value of 6.9% in tasks D16 and D14 under the ageing conditions t_s=150°C and τ_s=12 hours. In the remaining experiments for these ageing conditions, A_{gt} was also at a similarly high level. In turn, the lowest values A_{gt}=3.5% were achieved in task D1 carried out for the conditions of supersaturation equalling t_p=540°C and τ_p=11 hours and ageing of t_s=200°C and τ_s=12 hours.

The maximal value HBW=132 was reached in task D10 with the extremely high values of ageing (t_s=200°C and τ_s=12 hrs) and supersaturation (t_p=490°C and τ_p=11 hrs). The lowest values of hardness HBW equalling 92.2 and 92.4 units were recorded in tasks D5 and D14, with the ageing time of 4 and 12 hours at 150°C. In both cases, supersaturation occurred at 540°C and lasted 1 hour and 11 hours.

3.3. Optimization of thermal treatment parameters

The optimization of the thermal treatment T6 parameter settings was carried out in two stages. The steps within each stage are presented below.

3.3.1. Optimization (Stage I)

Based on the data from Table 4, regression equations (2) were developed for each of the analyzed mechanical properties (UTS, YS, A_{gt}, HBW) as a function of the thermal treatment T6 parameters (t_p, τ_p, t_s, τ_s) with the use of the Statgraphics Plus software. The regression equations and the parameter settings for the point determining the gradient vector sense are presented in Table 5.

The signs of the numbers (Latin *Signum*) in the resultant vector agree with the signs of the numbers in task D11. Based on the presented data, we can notice that only an increase of the ageing time t_s causes an increase of the UTS value, whereas an increase of τ_p, t_p and τ_s lowers the tensile strength. In the case of yield stress, an increase of both t_s and t_p causes an increase of its value, whereas an increase of τ_s and τ_p lowers the value of YS. For relative elongation A_{gt}, it was noticed that an increase of each of the input factors causes a reduction of its value. In turn, in the case of hardness HBW, an increase of the value of two factors, i.e. t_s and τ_p, causes an increase of its value. In turn, an increase of τ_s and t_p lowers the value of HBW.

Table 4.
Compilation of the results of the fundamental mechanical properties of the examined EN AC-46000 alloy – Stage I of optimization.

Runs	t_p, °C	τ_p, h	t_s, °C	τ_s, h	UTS, MPa	YS, MPa	A_{gt}, %	HBW	DSC
D0	515	6	175	8	352	309	4.5	130	1
D1	540	11	200	12	247	222	3.5	103	1
D2	490	11	200	12	310	272	4.1	115	0
D3	490	1	200	12	296	226	4.9	97	0
D4	540	1	200	12	310	252	4.7	115	1
D5	540	1	150	12	299	230	4.8	92	1
D6	540	11	150	12	245	210	4.3	109	1
D7	490	11	150	12	289	185	6.3	103	0
D8	490	1	150	12	310	213	5.4	112	0
D9	540	11	200	4	321	289	3.8	120	1
D10	490	11	200	4	333	291	4.3	132	0
D11	490	1	200	4	306	266	3.9	116	0
D12	540	1	200	4	330	305	4.3	127	1
D13	540	1	150	4	281	195	6.4	110	1
D14	540	11	150	4	225	197	6.9	92	1
D15	490	11	150	4	273	173	9.0	105	0
D16	490	1	150	4	297	180	6.9	107	0
				min	***225***	***173***	***3.5***	***92***	***0***
				max	***352***	***309***	***6.9***	***132***	***1***
				max-min	***127***	***136***	***3.4***	***40***	***1***

Table 5.
Regression equations and values of settings for the point determining the gradient vector sense

	UTS	YS	A_t	HBW
Y_i	UTS = 414.913+ -0.3905·t_p+ -2.3425·τ_p+ +0.59·t_s+ -0.9375·τ_s, MPa	YS = -108.295+ +0.23475·t_p+ -0.32375·τ_p+ +1.35075·t_s+ -1.36094 ·τ_s, MPa	A_t = 15.5826+ -0.007675·t_p+ -0.026125·τ_p + -0.033925·t_s + -0.0685938·τ_s, %	HBW = 101.311+ -0.047·t_p+ -0.035·τ_p+ -0.237·t_s+ -0.98125·τ_s
Settings (Inputs) determining the sense of the gradient vector	t_p=490°C τ_p=1 h t_s=200°C τ_s=4 h	t_p=540°C τ_p=1 h t_s=200°C τ_s=4 h	t_p=490°C τ_p=1 h t_s=150°C τ_s=4 h	t_p=540°C τ_p=1 h t_s=200°C τ_s=4 h

∇_{medium}=(-0.210425, -2.657375, 2.143825, -3.965627) signum in ∇_{medium}=(-,-,+,-) in agreement with D11 (Table 3)

To compare the obtained response values of the object, it was necessary to normalize the mechanical properties and the DCS indicator. The stimulant and destimulant values were determined to assume values from zero to one, as shown in Table 5. This table also presents the calculated values of the objective function Fo for each experiment. The maximum value of the objective function was achieved for task D10, reaching 3.945 (highlighted in yellow in Table 6).

Owing to the determined objective function value Fo, it was possible to determine the sense of the gradient vector which will be directed towards experiment D10. The discrepancy in the identification of the gradient vector sense of the most intensive changes in the object's response to the given inputs (task D11 Table 5) is connected with the fact that, at the first optimization stage, during the determination of the equations of the planes (2) on which the particular gradient vectors are located, the DSC coefficient is not taken into consideration, which does take place at the stage of determining the maximum of the objective function Fo (Table 6).

Table 6.
Normalization of the mechanical properties (stimulants) and the DPO index (destimulant): nUTS, nYS, nA_{gt}, nHB, nDCS and the objective function value Fo

Runs	t_p, °C	τ_p, h	t_s, °C	τ_s, h	nUTS	nYS	nA_{gt}	nHBW	nDSC	Fo
D0	515	6	175	8	1.00	1.00	0.31	0.95	0.00	3.26
D1	540	11	200	12	0.17	0.36	0.00	0.27	0.00	0.80
D2	490	11	200	12	0.67	0.73	0.17	0.57	1.00	3.14
D3	490	1	200	12	0.56	0.39	0.40	0.13	1.00	2.48
D4	540	1	200	12	0.67	0.58	0.34	0.57	0.00	2.17
D5	540	1	150	12	0.58	0.42	0.39	0.00	0.00	1.39
D6	540	11	150	12	0.16	0.27	0.25	0.42	0.00	1.09
D7	490	11	150	12	0.50	0.08	0.82	0.27	1.00	2.68
D8	490	1	150	12	0.67	0.29	0.56	0.50	1.00	3.02
D9	540	11	200	4	0.75	0.85	0.09	0.70	0.00	2.40
D10	490	11	200	4	0.85	0.87	0.22	1.00	1.00	3.95
D11	490	1	200	4	0.64	0.68	0.13	0.60	1.00	3.05
D12	540	1	200	4	0.83	0.97	0.23	0.87	0.00	2.90
D13	540	1	150	4	0.44	0.16	0.85	0.45	0.00	1.89
D14	540	11	150	4	0.00	0.18	0.99	0.01	0.00	1.18
D15	490	11	150	4	0.38	0.00	0.73	0.32	1.00	2.43
D16	490	1	150	4	0.57	0.05	1.00	0.37	1.00	2.99
									max=	3.95

Based on the presented considerations, it was assumed that task D10 would be the one to ultimately determine the direction and sense of the gradient vector anchored in task D0. The gradient vectors for the object responses (Yi) to the given inputs allow

optimization for single criteria, maximizing one of the responses of UTS, YS, A_{gt} or HBW.

The idea of presenting the gradient vector anchored in task D0 and directed towards task D10 in a graphic form showing the distribution of experiments in a coordinate system posed difficulties due to the inability to place four input factors on four coordinate axes. In order to provide an approximate graphical representation, a slightly inclined coordinate system was created based on the first three inputs (tp, τp, ts), whereas the axis representing the fourth input τs was placed above that coordinate system, which has been shown in Fig. 11.

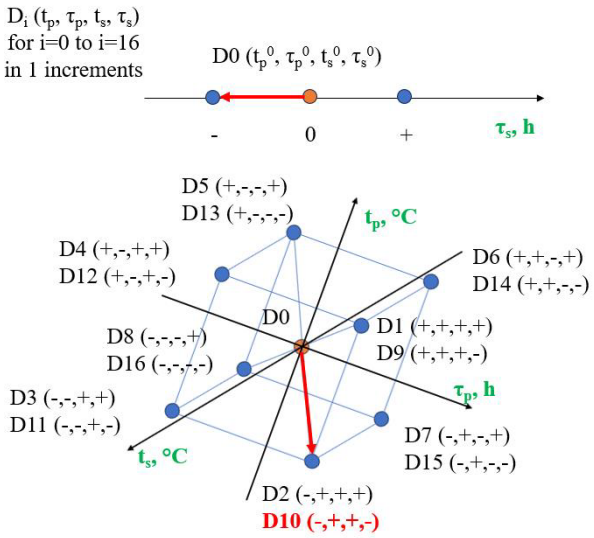

Fig. 11. Position of the gradient vector $\overrightarrow{D0D10}$ in the spatial model of the experiment plan

3.3.2. Optimization (Stage II)

Along the determined gradient vector, new experiments were established: D17, D18, D19, and D20, presented in Fig. 12. A compilation of the conditions for conducting thermal treatment T6 and the values of the output quantities Y_i for the experiments from the second step of optimization have been presented in Table 7.

In the regression model (5) of the mechanical properties Yi, there are 11 coefficients a_i (for i=0–10 at the distance of 1). In order to determine them, the tasks along the gradient vector D0, D17, D18, D10, D19, D20 were used, as well as the tasks from Stage I of optimization for which DSC=0 (no deformation of the cast's surface after thermal treatment).

Table 8 presents the regression models for the outputs Y_i (UTS, YS, A_t, HBW) in the experiments, the selection method as well as the statistical parameters, such as: α, $F_{\_cri}$, $F_{\_model}$, $p_{\_value}$, R^2, SEE, MAE. The presented regression models are significant ($F_{\_model}>F_{\_cri}$) and so are the coefficients a_i in the equations ($p_{\_value}$ $a_i\leq\alpha$). The models describe over 83.6% ($R^2>83.6\%$) of experimental cases at the assumed confidence level α=0.05. They characterize in a low standard deviation SEE and a small error MAE.

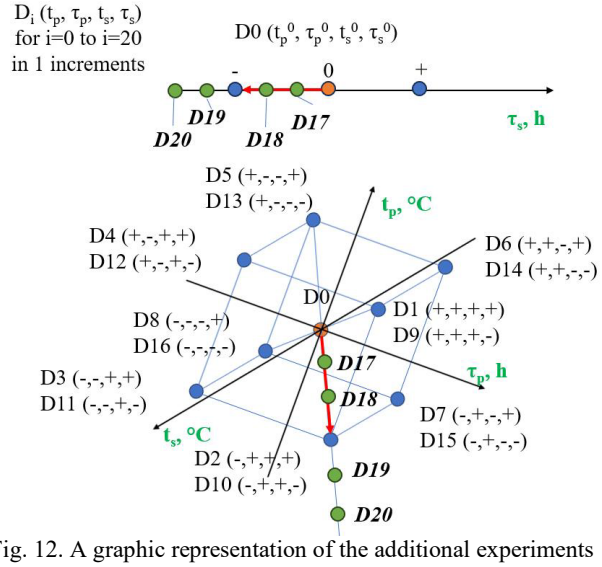

Fig. 12. A graphic representation of the additional experiments D17–D20 for the second stage of optimization

3.4. Simulation of property Y_i of alloy EN AC-46000 after thermal treatment T6

To determine the optimized parameters of the processes of supersaturation (t_p, τ_p) and ageing (t_s, τ_s), the previously elaborated regression equations were used (Tab. 8) and, based on them, the predicted values of mechanical properties were calculated for the considered time and temperature scope of both processes.

Tables 9–12 show the calculation values of the properties UTS, YS, A_{gt}, HBW determined based on the regression equations (Table 8). These functions were tabulated within the variability scope of the input factors X_i in the following scopes:

- supersaturation: t_p=490–540°C with the step of 5°C, τ_p=1–11 with the step of 1 h,
- ageing: t_s=150–200°C with the step of 5°C, τ_s=4–12 with the step of 1 h.

Table 7.
Compilation of the results of the fundamental mechanical properties of the examined EN AC-46000 alloy – Stage II of optimization

X_i		t_p, °C	τ_p, h (min.)	t_p, °C	τ_p, h (min.)	Stimulants				Destimulant
Range X_i		473–515	6–14(20)	175–217	1(20)–8	UTS, MPa	YS, MPa	A_{gt}, %	HBW	DCS 1 – Yes, 0 – No
δX_i		8.3	1(40)	8.3	1(20)					
Runs	D17	506.7	7(40)	183.3	6(40)	330	296	4.5	128	0
	D18	498.3	9(20)	191.7	5(20)	328	286	4.2	128	0
	D19	481.7	12(40)	208 3	2(40)	316	285	4.2	126	0
	D20	473.3	14(20)	216.7	1(20)	309	272	4.1	115	0

Table 8.
Regression models for outputs Y_i (UTS, YS, A_{gt}, HBW) in the experiment, selection method, statistical parameters: α, $F_{\_cri}$, $F_{\_model}$, $p_{\_value}$, R^2, SEE, MAE

	UTS		YS		A_{gt}		HBW	
Selection method	backward		backward		forward		backward	
Level α	0.05		0.05		0.05		0.05	
$F_{\_cri}$	2.92		2.92		2.63		2.92	
$F_{\_model}$	20.03		1374.83		56.17		18.97	
$p_{\_value}$	a_0	0.0012	a_2	0.0011	a_0	0.0000	a_0	0.0163
	a_3	0.0001	a_3	0.0000	a_6	0.0000	a_1	0.0181
	a_4	0.0260	a_4	0.0116	–		a_3	0.0098
	a_5	0.0046	a_6	0.0000	–		a_4	0.0226
	a_6	0.0001	a_8	0.0006	–		a_5	0.0098
	a_8	0.0045	a_{10}	0.0091	–		a_6	0.0094
	a_{10}	0.0247	–		–		a_8	0.0068
	–		–		–		a_{10}	0.0129
R^2	95.24		99.92		83.62		96.37	
SEE	6.46		10.10		0.41		3.38	
MAE	2.50		5.72		0.29		2.01	
Y_i	$UTS=230.713-5.60486\cdot t_s+$ $+10.8921\cdot t_s+$ $-0.0259061\cdot t_p\cdot\tau_p+$ $+0.0122567\cdot t_p\cdot t_s+$ $+0.0704194\cdot\tau_p\cdot t_s+$ $-0.0610321\cdot t_s\cdot\tau_s$, MPa		$YS=-19.1724\cdot\tau_p+$ $-8.17416\cdot t_s+12.1692\cdot\tau_s+$ $+0.0192869\cdot t_p\cdot t_s+$ $+0.11304\cdot t_p\cdot\tau_s+$ $-0.07119\cdot t_s\cdot\tau_s$, MPa		$A_t=11.6281+$ $-0.0000753491\cdot t_p\cdot t_s$, %		$HBW=2852.23+$ $-5.67504\cdot t_p-17.8064\cdot t_s+$ $+6.63258\cdot\tau_s+$ $-0.0134822\cdot t_p\cdot\tau_p+$ $+0.0368442\cdot t_p\cdot t_s+$ $+0.0403744\cdot\tau_p\cdot t_s+$ $-0.0429665\cdot t_s\cdot\tau_s$	

Table 9.
Calculations of the objective function value $UTS=f(t_p, \tau_p, t_s, \tau_s)$ (Table 8) for the parameters **t_s=200°C and τ_s=4 h**

t_p, °C \ τ_p, h	1	2	3	4	5	6	7	8	9	10	**11**
490	307	308	310	311	313	314	315	317	318	320	321
495	319	320	322	323	324	326	327	328	329	331	332
500	331	332	334	335	336	337	338	339	340	342	343
505	343	344	345	346	347	348	349	350	351	352	353
510	356	356	357	358	359	360	361	362	363	363	364
515	368	368	369	370	371	371	372	373	374	374	375
520	380	380	381	382	382	383	384	384	385	385	386
525	392	392	393	393	394	394	395	395	396	396	397
530	404	404	405	405	406	406	406	407	407	407	408
535	416	416	417	417	417	417	418	418	418	418	418
540	428	428	429	429	429	429	429	429	429	429	429

Table 10.
Calculations of the objective function value YS=f(t_p, τ_p, t_s, τ_s) (Table 8) for the parameters **t_s=200°C and τ_s=4 h**

τ_p, h / t_p, °C	1	2	3	4	5	6	7	8	9	10	**11**
490	250	254	257	261	264	268	271	275	278	281	285
495	270	273	277	280	284	287	290	294	297	301	304
500	289	293	296	299	303	306	310	313	317	320	323
505	308	312	315	319	322	326	329	332	336	339	343
510	328	331	335	338	341	345	348	352	355	359	362
515	347	350	354	357	361	364	368	371	374	378	381
520	366	370	373	377	380	383	387	390	394	397	401
525	386	389	392	396	399	403	406	410	413	416	420
530	405	408	412	415	419	422	425	429	432	436	439
535	424	428	431	434	438	441	445	448	452	455	458
540	443	447	450	454	457	461	464	467	471	474	478

Table 11.
Calculations of the objective function value A_{gt}=f(t_p, τ_p, t_s, τ_s) (Table 8) for the parameters **t_s=200°C and τ_s=4 h**

τ_p, h / t_p, °C	1	2	3	4	5	6	7	8	9	10	**11**
490	4.2	4.2	4.2	4.2	4.2	4.2	4.2	4.2	4.2	4.2	4.2
495	4.2	4.2	4.2	4.2	4.2	4.2	4.2	4.2	4.2	4.2	4.2
500	4.1	4.1	4.1	4.1	4.1	4.1	4.1	4.1	4.1	4.1	4.1
505	4.0	4.0	4.0	4.0	4.0	4.0	4.0	4.0	4.0	4.0	4.0
510	3.9	3.9	3.9	3.9	3.9	3.9	3.9	3.9	3.9	3.9	3.9
515	3.9	3.9	3.9	3.9	3.9	3.9	3.9	3.9	3.9	3.9	3.9
520	3.8	3.8	3.8	3.8	3.8	3.8	3.8	3.8	3.8	3.8	3.8
525	3.7	3.7	3.7	3.7	3.7	3.7	3.7	3.7	3.7	3.7	3.7
530	3.6	3.6	3.6	3.6	3.6	3.6	3.6	3.6	3.6	3.6	3.6
535	3.6	3.6	3.6	3.6	3.6	3.6	3.6	3.6	3.6	3.6	3.6
540	3.5	3.5	3.5	3.5	3.5	3.5	3.5	3.5	3.5	3.5	3.5

Since, starting from the temperature t_p=515°C, surface deformations (DSC=1) appeared in the cast after the thermal treatment T6, the values of the determined properties Y_i for the temperature scope t_p=515–540° were excluded from the calculations of the objective function Fo. In Tables 8–12, the area excluded from the calculations is highlighted with a grey background in the respective cells.

The obtained data were normalized to determine the maximal objective function value Fo, indicating the simultaneously possible highest values of all the output factors Y_i. The objective function was calculated, and its maximum value has been presented in Table 13 (highlighted in green). It equalled 1.9818 for the saturation parameters t_p=510°C and τ_p=11 h as well as the ageing parameters t_s=200°C and τ_s=4 h.

Table 12.
Calculations of the objective function value HBW_t=f(t_p, τ_p, t_s, τ_s) (Table 8) for the parameters **t_s=200°C and τ_s=4 h**

τ_p, h / t_p, °C	1	2	3	4	5	6	7	8	9	10	**11**
490	115	116	118	119	120	122	123	125	126	128	129
495	123	124	126	127	129	130	131	133	134	136	137
500	131	133	134	135	137	138	139	141	142	143	145
505	140	141	142	144	145	146	147	149	150	151	152
510	148	149	151	152	153	154	155	157	158	159	160
515	157	158	159	160	161	162	163	165	166	167	168
520	165	166	167	168	169	170	171	172	174	175	176
525	173	174	175	176	177	178	179	180	181	182	183
530	182	183	184	185	186	186	187	188	189	190	191
535	190	191	192	193	194	195	195	196	197	198	199
540	199	199	200	201	202	203	203	204	205	206	207

Table 13.
Calculations of the highest objective function value Fo for the parameters **t_p=510°C**, **τ_p=11 h**, **t_s=200°C** and **τ_s=4 h** for nDSC=1

τ_p, h / t_p, °C	1	2	3	4	5	6	7	8	9	10	**11**
490	0.98	1.01	1.04	1.07	1.11	1.14	1.17	1.20	1.24	1.27	1.30
495	1.16	1.19	1.22	1.25	1.29	1.32	1.35	1.38	1.41	1.44	1.47
500	1.34	1.37	1.40	1.43	1.46	1.49	1.52	1.55	1.58	1.61	1.64
505	1.53	1.56	1.58	1.61	1.64	1.67	1.70	1.73	1.76	1.78	1.81
510	1.71	1.74	1.77	1.79	1.82	1.85	1.87	1.90	1.93	1.95	1.98

4. Summary

The aim of the work was to develop the optimal technological parameters for the thermal treatment of products made from the EN AC-46000 alloy, produced with the use of the vacuum-assisted pressure casting technology. For the casts made by means of this technology, both after aging and for casts without the thermal treatment T6, the fundamental mechanical properties were determined, i.e.: tensile strength (UTS), yield stress (YS), relative elongation at maximum load (A_{gt}), and hardness (HBW).

Among the casts subjected to the T6 treatment, the highest values of the examined mechanical properties were as follows: tensile strength UTS=352 MPa (Task D0), yield stress YS=309 MPa (also task D0), relative elongation A_{gt}=6,9% (tasks D14 and D16), and hardness HBW=132 (task D10). The maximal values were reached in different experiments, that is with the application of different temperatures and times of supersaturation and ageing.

In comparison, the values of the same properties in the case of a cast without a thermal treatment T6 equalled: UTS=254 MPa, Ys=141 MPa, A_{gt}=4,0% and HBW=114, respectively.

Additionally, a visual assessment of the cast surface was taken into account in order to check for the presence of deformations (DCS). It was observed that such deformations occur in casts where the saturation process was conducted at temperatures of 515°C and higher (Tables 4 and 6).

Selected samples for the experiments conducted under the same ageing conditions (t_s=200°C i τ_s=12 h) and extreme conditions of the saturation process, that is both the maximum and minimum temperature and time, were subjected to microstructural tests. This analysis also included a sample from the central point of the experiment plan for the first step of optimization (task D0) and a sample from a cast that was not subjected to thermal treatment. The non-heat-treated alloy characterized in a microstructure composed of fine-grained α_{Al}+β(Si) eutectic, primary α_{Al} phase precipitates, and intermetallic phases (Fig. 8a). In turn, in samples subjected to thermal treatment, coagulation and coalescence of silicon precipitates was generally observed (Fig. 8b, 9a,b and 10b). An exception is the sample for which solution annealing occurred at the minimum temperature t_p=490°C and time τ_p=1 h. In this case, no coagulation and coalescence processes of silicon precipitates were observed (Fig. 10a).

In order to determine the optimal parameters for the processes of solution annealing (tp and τp) and ageing (t_s and τ_s), a two-step experimental plan was developed based on the Box-Wilson optimization method. This method involves searching for the minimum or maximum response of the object to the given inputs. In addition to the experiment plan, the first stage also included determining the position of the vector of the most intensive changes in the object's response. This experiment consisted of 17 trials (Table 3). The equations of the gradient vector plane for each output of the object were also determined. Subsequently, the values of stimulants and destimulants were normalized, allowing for the determination of the maximum value of the objective function, and thus the position of the gradient vector. Considering the DCS indicator, the highest value of the objective function was obtained for experiment D10 (Fig. 4).

The second stage of optimization involved a more precise localization of the optimum by conducting a larger number of experiments in the designated direction of optimization. Additional experiments D17, D18, D19, and D20 were determined, for which the mechanical properties were measured (Table 6). Next, the normalization of the values of stimulants and destimulants was also performed, and the maximum value of the objective function Fc was determined (Table 13). The aim was to establish a regression function with one extremum. To determine all the terms of this equation, the method of stepwise multiple regression analysis was used in the statistical software Statgraphics Plus. To achieve this goal, the values of stimulants and destimulants for the new experiments were entered into the program. This resulted in significant, selected regression equations with significant coefficients (Table 8). These equations were used to conduct a simulation of the mechanical properties for the specific parameters of supersaturation and ageing. This made it possible to identify the local extremes of the examined mechanical properties. The highest value UTS=364 MPa was obtained for the supersaturation parameters of t_p=510°C and τ_p=11 h and for the ageing parameters of t_s=200°C and τ_s=4 h. In turn, the highest value YS=362 MPa, was achieved for the supersaturation parameters of t_p=510°C and τ_p=11 h and the ageing parameters of t_s=200°C and τ_s=4 h. For A_{gt}, the highest obtained value was 6,1%, for the supersaturation parameters of t_p=490°C and τ_p=1–11 h and the ageing parameters of t_s=150°C and τ_s=4–12 h. The highest value for HBW equalled 160, for t_p=510°C and τ_p=11 hrs and t_s=200°C and τ_s=4 h.

Based on the simulated and then normalized values of the mechanical properties (Tables 9-12), the objective function was calculated (Table 13), which identified the optimized values for the parameters of the solution annealing and aging processes. The determined optimal values of the thermal treatment parameters are as follows: t_p=510°C, τ_p=11 h, t_s=200°C and τ_s=4 h (tab. 13). In turn, the mechanical properties for these parameters equalled: UTS=364 MPa (Tab. 9), YS=362 MPa (Tab. 10), A_{gt}=3,9% (Tab. 11) and HBW=160 (Tab. 12).

The validation of the response properties Y_i in the experiment for the optimized values X_i controlling the thermal treatment process T6 of the examined alloy EN AC-46000 was carried out. The microstructure of the alloy obtained because of the thermal

treatment performed for the optimized parameters of the component procedures has been shown in Fig. 13.

The presented microstructure consists of a solid solution matrix α_{Al}, silicon precipitates β(Si) and intermetallic phases. The presented data indicate that the silicon precipitates β(Si) visible on it have undergone the processes of coalescence and coagulation. In turn, the obtained mechanical properties in this case were as follows: UTS=355 MPa; YS=311 MPa; A_{gt}=4,1% and HBW =131.

Taking the above into account, it has been demonstrated that it is possible to effectively conduct thermal treatment in the form of precipitation hardening (T6) of pressure-cast aluminium alloys with vacuum assistance.

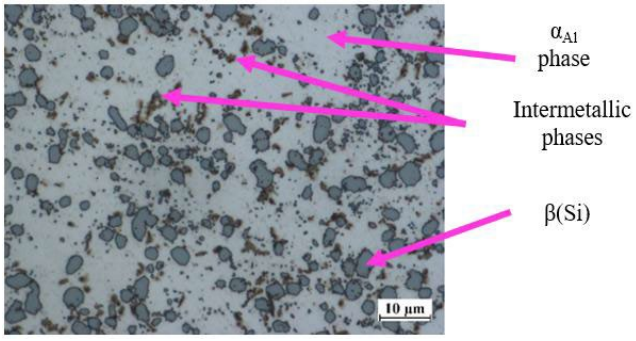

Fig. 13. Microstructure of alloy EN-AC 46000 for optimized thermal treatment parameters: t_p=510°C, τ_p=11 h, t_s=200°C and τ_s=4 h

5. Conclusions

The conclusions from the research presented in this work are described below.

1) The best measured mechanical properties for the experiments according to the experiment plan were as follows: UTS=352 MPa; YS=309 MPa; A_{gt}=6,9% and HBW=132.
2) Surface deformation of the cast occurred in experiments conducted at the solution annealing temperature of 515°C and higher.
3) The microstructure of the cast without thermal treatment characterized in a fine-grained α_{Al}+β(Si) eutectic, primary precipitates of α_{Al} phase and intermetallic phases of the type Al_2Cu, Mg_2Si as well as iron-manganese phases. In turn, coagulation and coalescence of silicon precipitates occurred in samples subjected to thermal treatment whose solution annealing time was 6 or 11 hours, or whose solution annealing temperature equalled a 540°C.
4) For the thermal treatment process T6 of alloy EN-AC 46000, the optimal set parameters were identified as follows: t_p=510°C, τ_p=11 h, t_s=200°C and τ_s = 4 h.
5) The results obtained from the simulation of the mechanical properties of the aluminium alloy for the optimized parameters of the saturation and aging processes were as follows: UTS=364 MPa, YS=362 MPa, A_{gt}=3.9%, HBW=160.
6) As a result of the validation conducted for the aluminium alloy subjected to thermal treatment T6, the following values of the fundamental mechanical properties were obtained: UTS=355 MPa, YS=311 MPa, A_{gt}=4.1%, HBW=131.
7) Taking the above into account, it has been demonstrated that it is possible to effectively carry out thermal treatment in the form of precipitation hardening (T6) of the pressure-cast EN AC-46000 aluminium alloy with vacuum assistance.

Acknowledgements

The research was conducted as part of a project funded by the National Centre for Research and Development, POIR.01.01.01-00-0008/20-00 titled ‘Development of an innovative technology for the production of pressure casts from aluminium alloys with enhanced quality parameters’.

References

[1] Farkoosh, A.R., Chen, X.G. & Pekguleryuz, M. (2015). Dispersoid strengthening of a high temperature Al–Si–Cu–Mg alloy via Mo addition. *Materials Science and Engineering*: A. 620, 181-189. https://doi.org/10.1016/j.msea.2014.10.004.
[2] Kim, H.Y., Han, S.W. & Lee, H.M. (2006). The influence of Mn and Cr on the tensile properties of A356–0.20Fe alloy. *Materials Letters*. 60(15), 1880-1883. https://doi.org/10.1016/j.matlet.2005.12.042.
[3] Elhadari, H.A., Patel, H.A., Chen, D.L. & Kasprzak, W. (2011). Tensile and fatigue properties of a cast aluminum alloy with Ti, Zr and V additions. *Materials Science and Engineering: A*. 528(24), 8128-8138. https://doi.org/10.1016/j.msea.2011.07.018.
[4] Li, Y., Yang, Y., Wu, Y., Wei, Z. & Liu, X. (2011). Supportive strengthening role of Cr-rich phase on Al–Si multicomponent piston alloy at elevated temperature. *Materials Science and Engineering*: *A*. 528(13-14), 4427-4430. https://doi.org/10.1016/j.msea.2011.02.047.
[5] Sjölander, E. & Seifeddine, S. (2010). The heat treatment of Al–Si–Cu–Mg casting alloys. *Journal of Materials Processing Technology*. 210(10), 1249-1259. https://doi.org/10.1016/j.jmatprotec.2010.03.020.
[6] Sjölander, E. & Seifeddine, S. (2011). Artificial ageing of Al–Si–Cu–Mg casting alloys. *Materials Science and Engineering*: A. 528(24), 7402-7409. https://doi.org/10.1016/j.msea.2011.06.036.
[7] Sjölander, E. & Seifeddine, S. (2010). Optimisation of solution treatment of cast Al–Si–Cu alloys. *Materials and Design*. 31(1), 44-S49. https://doi.org/10.1016/j.matdes.2009.10.035.
[8] Lumley, R.N., Gunasegaram, D.R., Gershenzon, M. & O’Donnell, R.G. (2010). Effect of alloying elements on heat treatment response of aluminium high pressure die castings. *International Heat Treatment and Surface Engineering*. 4(1), 25-32. https://doi.org/10.1179/174951409X12542264514004.
[9] Bonollo, F., Urban, J., Bonatto, B., & Botter, M. (2005). Gravity and low pressure die casting of aluminium alloys:

A technical and economical benchmark. *La Metallurgia Italiana*. 6, 23-32.
[10] Szymczak, T., Gumienny, G. & Pacyniak, T. (2014). Selected aspects of nitrogen refinement of Silumin 226. *Archives of Foundry Engineering*. 14(3), 99-102. https://doi.org/10.2478/afe-2014-0070.
[11] Ozhoga-Maslovskaja, O., Gariboldi, E. & Lemke, J. N. (2016). Conditions for blister formation during thermal cycles of Al–Si–Cu–Fe alloys for high pressure die-casting. *Materials and Design*. 92, 151-159. https://doi.org/10.1016/j.matdes.2015.12.003.
[12] Lumley, R.N., O'Donnell, R.G., Gunasegaram, D.R. & Givord, M. (2007). Heat treatment of high-pressure die castings. *Metallurgical and Materials Transactions A.* 38(12), 2564-2574. https://doi.org/10.1007/s11661-007-9285-4.
[13] Lumley, R.N., Deeva, N. & Gershenzon, M. (2010). The optimization of strength and ductility in heat treated ADC12 alloys. In 12th International Conference on Aluminium Alloys, 5-9 September 2010 (pp. 2197-2202). The Japan Institute of Light Metals.
[14] Yang, H., Ji, S. & Fan, Z. (2015). Effect of heat treatment and Fe content on the microstructure and mechanical properties of die-cast Al–Si–Cu alloys. *Materials and Design*. 85, 823-832. https://doi.org/10.1016/j.matdes.2015.07.074.
[15] PN-EN 1706:2020-10 Aluminium and Aluminium Alloys - Castings - Chemical Composition and Mechanical Properties.
[16] PN-EN ISO 6892-1:2020-05 Metals – Tensile Test – Part 1: Room Temperature Test Method. (in Polish).
[17] PN-EN ISO 6506-1:2014-12 Metallic Materials – Brinell Hardness Test – Part 1: Test Method. (in Polish).
[18] Belov, N.A., Eskin, D.G. & Aksenov, A. (2005) *Multicomponent Phase Diagrams. Applications for commercial aluminum alloy*. Oxford: Elsevier.
[19] Glazoff, M., V., Khvan, A. & Zolotorevsky, V.S. (2018). *Casting Aluminum Alloys. Their physical and mechanical metallurgy.* Butterworth-Heinemann.
[20] Belov, N., Aksenov, A.A. & Eskin, D.G. (2002). *Iron in Aluminum Alloys: Impurity and alloying elements*. London: CRC Press.
[21] Szymczak, T. (2019). *The Influence of Cr, Mo, V, and W on the Crystallization Process and Mechanical Properties of Hypoeutectic Silumins.* Łódź: Lodz University of Technology Publishing House. (in Polish).
[22] Callegari, B., Lima, T.N. & Coelho, R.S. (2023). The influence of alloying elements on the microstructure and properties of Al-Si-based casting alloys: A review. *Metals.* 13(7), 1174, 1-36. https://doi.org/10.3390/met13071174.
[23] Kowalczyk, W., Dańko, R., Górny, M., Kawalec, M. & Burbelko, A. (2022). Influence of high-pressure die casting parameters on the cooling rate and the structure of EN-AC 46000 alloy. *Materials*. 15(16), 5702, 1-16. https://doi.org/10.3390/ma15165702.
[24] Bolibruchová, D., Matejka, M., Michalcová, A., & Kasińska, J. (2020). Study of natural and artificial aging on AlSi9Cu3 alloy at different ratios of returnable material in the batch. *Materials*. 13(20), 4538, 1-16. https://doi.org/10.3390/ma13204538.
[25] Ruyao Wang, Weihua Lu. (2016). Hypereutectic Al-Si alloy with completely nodular eutectic silicon: microstructure and process. *International Journal of Materials Science and Applications*. 5(6), 277-283. https://doi.org/10.11648/j.ijmsa.20160506.17.
[26] Jarco, A.; Pezda, J. (2021). Effect of heat treatment process and optimization of its parameters on mechanical properties and microstructure of the AlSi11(Fe) Alloy. *Materials*. 14(9), 2391, 1-20. https://doi.org/10.3390/ma14092391.
[27] Pietrowski, S. (2001). *Al-Si alloys*. Łódź: Lodz University of Technology Publishing House. (in Polish).